Novel wideband microwave polarization network using a fully-reconfigurable photonic waveguide interleaver with a two-ring resonator-assisted asymmetric Mach-Zehnder structure

Leimeng Zhuang,[1,*] Willem Beeker,[2] Arne Leinse,[2] René Heideman,[2] Paulus van Dijk,[3] and Chris Roeloffzen[1,3]

[1]*Telecommunication Engineering group, University of Twente, PO Box 217, Enschede, 7500 AE, The Netherlands*
[2]*LioniX BV, PO Box 456, Enschede, 7500 AL, The Netherlands*
[3]*SATRAX BV, PO Box 456, Enschede, 7500 AL, The Netherlands*
[*]*l.zhuang@ewi.utwente.nl*

Abstract: We propose and demonstrate a novel wideband microwave photonic polarization network for dual linear-polarized antennas. The polarization network is based on a waveguide-implemented fully-reconfigurable optical interleaver using a two-ring resonator-assisted asymmetric Mach-Zehnder structure. For microwave photonic signal processing, this structure is able to serve as a wideband 2 × 2 RF coupler with reconfigurable complex coefficients, and therefore can be used as a polarization network for wideband antennas. Such a device can equip the antennas with not only the polarization rotation capability for linear-polarization signals but also the capability to operate with and tune between two opposite circular polarizations. Operating together with a particular modulation scheme, the device is also able to serve for simultaneous feeding of dual-polarization signals. These photonic-implemented RF functionalities can be applied to wideband antenna systems to perform agile polarization manipulations and tracking operations. An example of such a interleaver has been realized in TriPleX waveguide technology, which was designed with a free spectral range of 20 GHz and a mask footprint of smaller than 1 × 1 cm. Using the realized device, the reconfigurable complex coefficients of the polarization network were demonstrated with a continuous bandwidth from 2 to 8 GHz and an in-band phase ripple of smaller than 5 degree. The waveguide structure of the device allows it to be further integrated with other functional building blocks of a photonic integrated circuit to realize on-chip, complex microwave photonic processors. Of particular interest, it can be included in an optical beamformer for phased array antennas, so that simultaneous wideband beam and polarization trackings can be achieved photonically. To our knowledge, this is the first-time on-chip demonstration of an integrated microwave photonic polarization network for dual linear-polarized antennas.

OCIS codes: (060.2360) Fiber optic links and subsystems; (060.5625) Radio frequency photonics; (070.6020) Continuous optical signal processing; (130.3120) Integrated optics devices; (350.4010) Microwave.

References and links

1. J. Capmany and D. Novak, "Microwave photonics combines two worlds," Nat. Photonics 1(6), 319–330 (2007).
2. J. Yao, "Microwave photonics," J. Lightwave Technol. 27(3), 314–335 (2009).
3. I. Gasulla, J. Lloret, J. Sancho, S. Sales, and J. Capmany, "Recent breakthroughs in microwave photonics," IEEE Photonics J. 3(2), 311–315 (2011).

#181159 - $15.00 USD Received 4 Dec 2012; revised 23 Jan 2013; accepted 23 Jan 2013; published 1 Feb 2013

4. J. Capmany, I. Gasulla, and S. Sales, "Microwave photonics: Harnessing slow light," Nat. Photonics 5(12), 731–733 (2011).
5. D. A. I. Marpaung, C. G. H. Roeloffzen, R. G. Heideman, A. Leinse, S. Sales, and J. Capmany, "Integrated microwave photonics," Laser Photonics Rev., DOI:10.1002/lpor.201200032 (2013).
6. J. Sancho, J. Bourderionnet, J. Lloret, S. Combrié, I. Gasulla, S. Xavier, S. Sales, P. Colman, G. Lehoucq, D. Dolfi, J. Capmany, and A. De Rossi, "Integrable microwave filter based on a photonic crystal delay line," Nat. Commun. 3(9), (2012).
7. M. Burla, D. A. I. Marpaung, L. Zhuang, C. G. H. Roeloffzen, M. R. Khan, A. Leinse, M. Hoekman, and R. G. Heideman, "On-chip CMOS compatible reconfigurable optical delay line with separate carrier tuning for microwave photonic signal processing," Opt. Express 19(22), 21475–21484 (2011).
8. N. N. Feng, P. Dong, D. Feng, W. Qian, H. Liang, D. C. Lee, J. B. Luff, A. Agarwal, T. Banwell, R. Menendez, P. Toliver, T. K. Woodward, and M. Asghari, "Thermally-efficient reconfigurable narrowband RF-photonic filter," Opt. Express 18(24), 24648–24653 (2010).
9. M. H. Khan, H. Shen, Y. Xuan, L. Zhao, S. Xiao, D. E. Leaird, A. M. Weiner, and M. Qi, "Ultrabroad-bandwidth arbitrary radiofrequency waveform generation with a silicon photonic chip-based spectral shaper," Nat. Photonics 4(2), 117–122 (2010).
10. A. Meijerink, C. G. H. Roeloffzen, R. Meijerink, Leimeng Zhuang, D. A. I. Marpaung, M. J. Bentum, M. Burla, J. Verpoorte, P. Jorna, A. Hulzinga, and W. van Etten, "Novel ring resonator-based integrated photonic beamformer for broadband phased-array antennas-Part I: design and performance analysis," J. Lightwave Technol. 28(1), 3–18 (2010).
11. L. Zhuang, C. G. H. Roeloffzen, A. Meijerink, M. Burla, D. A. I. Marpaung, A. Leinse, M. Hoekman, R. G. Heideman, and W. C. van Etten, "Novel ring resonator-based integrated photonic beamformer for broadband phased-array antennas-Part II: experimental prototype," J. Lightwave Technol. 28(1), 19–31 (2010).
12. M. Ferrera, Y. Park, L. Razzari, B. E. Little, S. T. Chu, R. Morandotti, D. J. Moss, and J. Azaña, "On-chip CMOS-compatible all-optical integrator," Nat. Commun. 1(29) (2010).
13. F. Liu, T. Wang, L. Qiang, T. Ye, Z. Zhang, M. Qiu, and Y. Su, "Compact optical temporal differentiator based on silicon microring resonator," Opt. Express 16(20), 15880–15886 (2008).
14. D. A. I. Marpaung, C. G. H. Roeloffzen, A. Leinse, and M. Hoekman, "A photonic chip based frequency discriminator for a high performance microwave photonic link," Opt. Express 18(26), 27359–27370 (2010).
15. D. A. I. Marpaung, L. Chevalier, M. Burla, and C. G. H. Roeloffzen, "Impulse radio ultrawideband pulse shaper based on a programmable photonic chip frequency discriminator," Opt. Express 19(25), 24838–24848 (2011).
16. L. Zhuang, M. R. Khan, W. P. Beeker, A. Leinse, R. G. Heideman, and C. G. H. Roeloffzen, "Novel microwave photonic fractional Hilbert transformer using a ring resonator-based optical all-pass filter," Opt. Express 20(24), 26499–26510 (2012).
17. J. F. White, *High Frequency Techniques: An Introduction to RF and Microwave Engineering* (Wiley, 2004).
18. R. E. Collin, *Antennas and Radiowave Propagation* (McGraw-Hill, 1985).
19. C. K. Madsen and J. H. Zhao, *Optical Filter Design and Analysis* (Wiley, 1999).
20. C. J. Kaalund and G. Peng, "Pole-zero diagram approach to the design of ring resonator-based filters for photonic applications," J. Lightwave Technol. 22(6), 1548–1559 (2004).
21. Z. Wang, S. Chang, C. Ni, and Y. Chen, "A high-performance ultracompact optical interleaver based on double-ring assisted Mach-Zehnder interferometer," IEEE Photonics Lett. 19(14), 1072–1075 (2007).
22. R. G. Heideman, M. Hoekman, and E. Schreuder, "TriPleX-based integrated optical ring resonators for lab-on-a-chip and environmental detection," IEEE J. Sel. Top. Quantum Electron. 18(5), 1583–1596 (2012).
23. L. Zhuang, D. A. I. Marpaung, M. Burla, W. P. Beeker, A. Leinse, and C. G. H. Roeloffzen, "Low-loss, high-index-contrast Si_3N_4/SiO_2 optical waveguides for optical delay lines in microwave photonics signal processing," Opt. Express 19(23), 23162–23170 (2011).

1. Introduction

Microwave photonic (MWP) signal processing techniques have been advancing with ever-growing attentions and efforts in the recent decades [1, 2]. The rich bandwidth availability, electromagnetic interference immunity, high frequency capability, as well as the possibility of realizing RF systems with small size, weight, and power consumptions have brought such techniques to a strong competitive position, compared to the conventional all-electronics solutions. Next to the performances, MWP may also create novel RF functionalities and thereby enable new information and communication systems [3, 4]. More promisingly, the fast progress in photonic integration has started to establish a mature hardware platform for the realization of on-chip, complex MWP signal processors [5]. Same as in the electronics world, on-chip MWP signal processors feature higher robustness, more compact and greener systems, and more importantly, potentials of significant system cost reduction, which are of paramount significance for its proliferation and prosperity, especially when addressing various consumer applications.

Alongside the photonic integration, the implementation of desired RF functionalities is equally important for the potential booming of integrated MWP. In the last decade, various

#181159 - $15.00 USD Received 4 Dec 2012; revised 23 Jan 2013; accepted 23 Jan 2013; published 1 Feb 2013

RF functionalities have been demonstrated using MWP chips, where several salient works include spectral filters [6–8], arbitrary waveform generator [9], beamforming network [10], [11], integrator [12], differentiator [13], frequency discriminator [14], UWB pulse shaper [15], and etc. To continue this progressing pace, recently a waveguide-based optical interleaver was designed and fabricated. The fabricated optical interleaver uses two-ring resonator (RR)-assisted asymmetric Mach-Zehnder interferometer (MZI) structure and features full reconfigurability. It is able to serve as a wideband 2 × 2 RF coupler with reconfigurable complex coefficients. This RF functionality is achieved using the Hilbert transformer (HT) functionality of the RRs [16] and amplitude tapering capability of the optical couplers. Such RF couplers can be used in a wide range of applications [17]. Among them, one interesting practice is a polarization network for wideband dual linear-polarized (DLP) antennas [18]. The proposed device can equip the DLP antennas with not only polarization rotation capability for linear-polarization (LP) signals but also the capability to operate with and tune between two opposite circular polarizations (CPs), namely between left-hand circular polarization (LHCP) and right-hand circular polarization (RHCP). Operating together with a particular modulation scheme, the device is able to serve for simultaneous feeding of dual-polarization (DP) signals. These photonic-implemented RF functionalities can be applied to wideband antenna systems to perform agile polarization manipulations and tracking operations.

In this paper, we propose and demonstrate the RF coupler functionality implemented using the optical interleaver. In Section 2, the device principle is explained, followed by a discussion on its application as a polarization network for DLP antennas. Section 3 describes the waveguide technology and mask design of a fabricated device. Section 4 presents the device characterizations, where the measurements on design accuracy and the full reconfigurability of the optical interleaver are exhibited, followed by the demonstrations of complex coefficients for the RF coupler functionality. The conclusions of this paper are formulated in Section 5.

2. Device principle

2.1 Device structure and transfer functions

A schematic of an optical interleaver with a two-ring resonator (RR)-assisted asymmetric MZI structure is depicted in Fig. 1(a), where κ_n's and ϕ_n's express the optical power coupling coefficients and additional optical phase shifts, respectively. This structure consists of a 2 × 2 asymmetric MZI with both arms coupled to a RR. The RRs have the same roundtrip length, L_R, which is twice the length difference between the two arms of the MZI, ΔL.

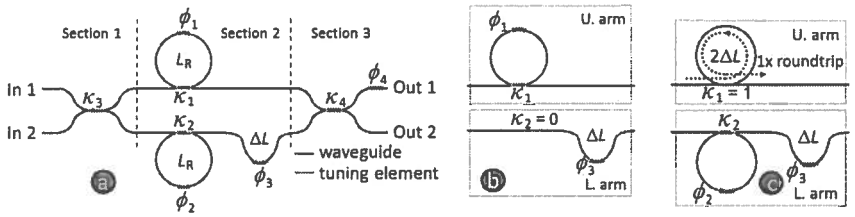

Fig. 1. (a) schematic of a waveguide-based 2 × 2 interleaver with a two-ring resonator-assisted asymmetric MZI structure; (b) equivalent circuit when the RR in the lower arm is decoupled; (c) equivalent circuit when the RR in the upper arm is full-coupled.

According to the signal processing principles of coherent optical filters such as MZIs and RRs [19], the transfer functions of such a structure can be derived from the z-transform expressions of its three sections shown in Fig. 1(a), which is given by

#181159 - $15.00 USD Received 4 Dec 2012; revised 23 Jan 2013; accepted 23 Jan 2013; published 1 Feb 2013

$$\mathbf{H} = \eta \begin{bmatrix} \sqrt{1-\kappa_4}\, e^{-j\phi_4} & -j\sqrt{\kappa_4}\, e^{-j\phi_4} \\ -j\sqrt{\kappa_4} & \sqrt{1-\kappa_4} \end{bmatrix} \begin{bmatrix} A_U(z) & 0 \\ 0 & A_L(z) \end{bmatrix} \begin{bmatrix} \sqrt{1-\kappa_3} & -j\sqrt{\kappa_3} \\ -j\sqrt{\kappa_3} & \sqrt{1-\kappa_3} \end{bmatrix} = \begin{bmatrix} H_{11} & H_{12} \\ H_{21} & H_{22} \end{bmatrix} \quad (1)$$

with
$$A_U(z) = \frac{\sqrt{1-\kappa_1} - r^2 z^{-2} e^{-j\phi_1}}{1 - \sqrt{1-\kappa_1}\, r^2 z^{-2} e^{-j\phi_1}} \quad (2)$$

and
$$A_L(z) = \frac{\sqrt{1-\kappa_2} - r^2 z^{-2} e^{-j\phi_2}}{1 - \sqrt{1-\kappa_2}\, r^2 z^{-2} e^{-j\phi_2}} \cdot r z^{-1} e^{-j\phi_3} \quad (3)$$

where $z = \exp(-j\nu)$ with $\nu = [-\pi, \pi]$ representing the normalized angular frequency with respect to the free spectral range (FSR) of the device ($\Delta f_{FSR} = 1/\Delta T = c_0/(\Delta L \cdot n_g)$ with ΔT the delay time for an optical path of ΔL, c_0 the speed of light in vacuum and n_g group index of the waveguide [19]), r is the amplitude transmission coefficient for an optical path of ΔL, and η is a complex coefficient which accounts for the general loss and phase shift introduced by the waveguides. Using Eqs. (1)-(3), one can derive the frequency responses between different inputs and outputs. It can be understood that the four transfer functions in Eq. (1) represent two pairs of 5th-order complementary spectral filters, which have five roots in their nominators and four in their denominators, namely five zeros and four poles in terms of digital signal processing concepts [19]. With properly chosen coefficients [20, 21], IIR Chebyshev type II filters with good interleaver performance can be implemented, which feature flat passbands, equal-ripple stopbands, and steep transitions simultaneously. To give an idea of the interleaver performance, the power transmission, phase and group delay responses of the filters for a typical setting of coefficients are depicted in Fig. 2.

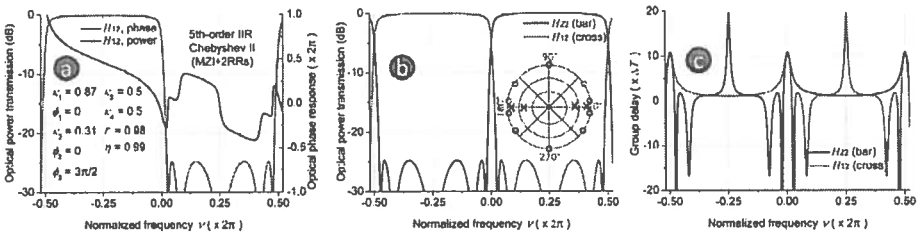

Fig. 2. Frequency responses of the interleaver for a typical setting of coefficients: (a) power transmission and phase responses of H_{12}, (b) zero-pole diagram and the complementary nature of the two outputs, (c) corresponding group delay responses.

2.2 Implementation of 2 × 2 RF coupler with reconfigurable complex coefficients

As described in the previous section, both arms of the asymmetric MZI are coupled to a RR, and $A_U(z)$ and $A_L(z)$ are the transfer functions of the upper and lower arm, respectively. It is important to notice that when the RR of the lower arm is decoupled from the arm ($\kappa_2 = 0$), $A_L(z)$ reduces to $rz^{-1}\exp(-j\phi_3)$, which describes a section consisting of a delay length of ΔL, an amplitude transmission coefficient r, and a phase shift of ϕ_3. The equivalent circuit is depicted in Fig. 1(b). At the same time, the RR of the upper arm can be properly set (for instance, $\kappa_1 = 0.87$) to provide a frequency response which represents a wideband MWP HT (RF phase shift of –90°) in cascade with a delay length of $L_R/2 = \Delta L$ [16]. This means that when MWP signals are split into the two arms, this setting will result in the same delay effect in both arms and at the same time introduce a RF 90°-phase-shift difference between them. To illustrate this operation, Fig. 3 depicts the optical and corresponding MWP phase responses derived from $A_U(z)$ and $A_L(z)$. Relative to the lower arm, the RF phase shift of the upper arm can also

#181159 - $15.00 USD Received 4 Dec 2012; revised 23 Jan 2013; accepted 23 Jan 2013; published 1 Feb 2013

be changed from −90° to 90°. However, this requires another setting of the two RRs, where the RR of the lower arm needs to be coupled and operates as a HT like the other RR in the former case (for instance, κ_2 = 0.87), while the RR of the upper arm operates as a simple delay line by means of full coupling (κ_1 = 1). The equivalent circuit is depicted in Fig. 1(c). Now, the upper arm provides an additional delay length equal to the roundtrip length of the RR, $L_R = 2\Delta L$, and thereby becomes ΔL longer than the lower arm. Consequently, this swaps the roles between the two arms, and therefore switches the relative RF phase shift of the upper arm from −90° to 90°. Furthermore, both RRs can be decoupled or full coupled ($\kappa_1 = \kappa_2$ = 0 or 1) to remove the resonance effect of the RRs and thereby render the device a regular asymmetric MZI. In this case, the two arms will only provide delay effects but no RF phase shift for MWP signal processing. Consequently, using the RF 90°-phase-shift difference enabled by the RRs and the amplitude tapering capability of the optical couplers, such an interleaver structure is able to serve as an MWP 2 × 2 RF coupler with reconfigurable complex coefficients.

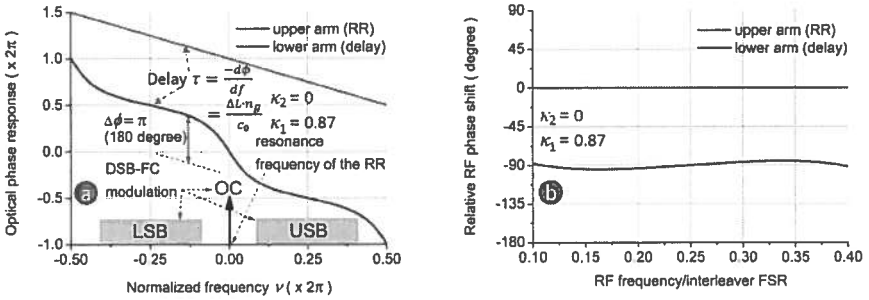

Fig. 3. Optical and corresponding MWP phase responses of the two arms: (a) the optical phase responses aligned with the MWP signals, (b) the achieved relative RF phase shift of the two arms.

2.3 Polarization network schemes for single-polarization signals

Wideband RF couplers are desired in numerous applications [17]. Among them, one interesting practice of the proposed MWP 2 × 2 RF coupler is a polarization network for wideband DLP antennas [18]. Here, we consider first the antenna radiations with only one single polarization (SP). In Fig. 4 and Fig. 5, the proposed schemes for transmit DLP antennas radiating CP and LP signals are depicted respectively. In the schemes, the Mach-Zehnder modulators (MZMs) are considered for the encoding of RF inputs on the optical carrier. As shown in Fig. 4, when the modulated signals are equally divided into the two arms by setting κ_3 = 0.5 and κ_4 = 0 (the possible signal amplitude difference due to the loss difference between the two arms can be compensated by adjusting κ_3), and the RRs are set as described in the previous section, the X antenna component will be characterized by equal amplitude and −90°(90°)-phase difference with respect to Y antenna component, which corresponds to the radiation of RHCP(LHCP) signals. Alternatively, when the RF input is fed in-phase to the antennas as shown in Fig. 5 with κ_3 = 0 and both RRs decoupled, LP signals are achieved. Then, by varying κ_4, the amplitude ratio between the two antenna components can be adjusted accordingly, resulting in polarization rotations. However, in this case, the photonic device is not able to feed the two antenna components with two opposite phases as desired for the achievement of a full polarization rotation range of 360° (arbitrary angle in the antenna plane). Therefore, an additional electrical polarity switching functionality as indicated in Fig. 5 is suggested to overcome this drawback. Alternatively, it is also possible to achieve this full rotation range by using a particular modulation scheme associated with full coherent optical processing. The discussion on this will be given in the next section, in

#181159 - $15.00 USD Received 4 Dec 2012; revised 23 Jan 2013; accepted 23 Jan 2013; published 1 Feb 2013

combination with the proposed polarization network schemes for DP signals. On the other hand, the reception of SP signals can be achieved by simply inversing the processings of the schemes described above, namely by swapping the MZMs and photodetectors (PDs). In this case, two arms of the polarization network are connected to two MZMs separately, and two independent optical carriers (assuming they are spectrally further apart than RF signal bandwidth) are assigned to the two antenna components. Then, the RF signals from the two antenna components will be processed by the polarization network in a parallel manner until the output of the PD. It is straightforward to deduce that when the signal polarization (RHCP, LHCP, or LP) matches the setting of the RRs and optical couplers as for the transmit antennas, the polarization network compensate the amplitude and phase difference of the two antenna components, so that the received RF signals from the two antenna components will add up constructively at the output of the PD.

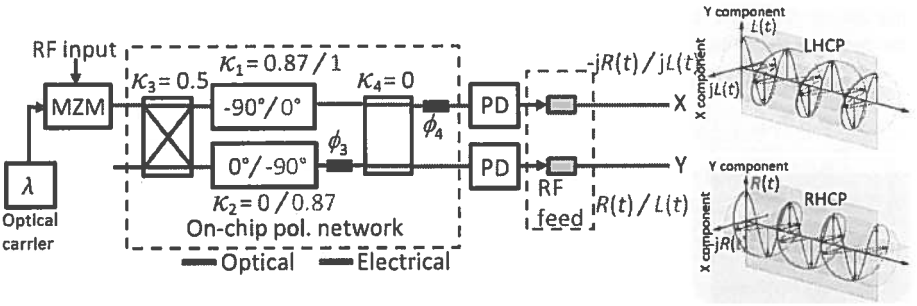

Fig. 4. System schemes for transmit DLP antennas with CP signal radiations.

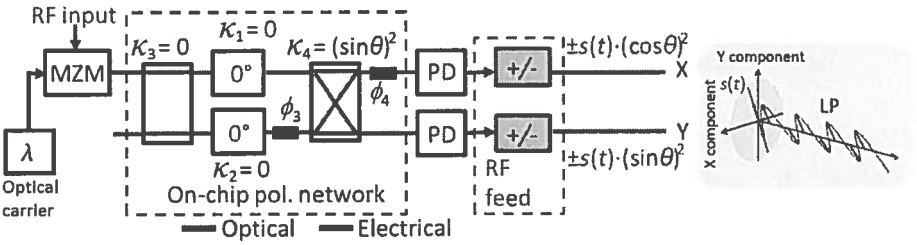

Fig. 5. System schemes for transmit DLP antennas with LP signal radiations.

2.4 Polarization network schemes for dual-polarization signals

To deal with two polarizations simultaneously, two polarization network schemes based on full coherent optical processing are proposed, which are depicted in Fig. 6 and Fig. 7. Here, the receive antennas are first considered. In these schemes, a single optical carrier is split into both arms of the polarization network. To maintain a stable manipulation of the optical phases, it is preferred that all the optical components including the optoelectronics are realized in waveguides and are integrated together either monolithically or by means of hybrid integration. This way, the system is free of optical fibers where optical phase stability is difficult to maintain due to its susceptibility to ambient disturbances. To explain the principles of this polarization network, illustrations of the optical signal processing in phase domain are presented in the insets of Fig. 6 and Fig. 7. In these schemes, a particular modulation scheme is used for the systems, where double sideband-suppressed carrier (DSB-SC) modulation is applied to one arm and double sideband-full carrier (DSB-FC) modulation to the other. The optical coupler and phase shifter before and after the MZMs guarantee that the optical carriers of the two arms are of 90°-optical phase difference and the ratio of the

#181159 - $15.00 USD Received 4 Dec 2012; revised 23 Jan 2013; accepted 23 Jan 2013; published 1 Feb 2013

signal amplitudes between the two arms are correctly adjusted according to the signal polarizations.

In case of CP signals, the LHCP (green) signals result in –90°-RF phase difference between the X and Y antenna component and simultaneously RHCP (red) signals 90°-RF phase difference. The depicts at (i) in Fig. 6 describes the signal phase relation between the two arms after modulation. Then, after experiencing the –90°-RF phase shift of the RR, the RHCP and LHCP signal of the upper arm are turned to be in phase and 180°-out of phase with the suppressed optical carrier, respectively, as depicted at (ii) in Fig. 6. Next, the optical coupler κ_3 splits the unsuppressed optical carrier in the lower arm into the two outputs of the polarization network and simultaneously guarantees that the two arms have equal RF amplitude contributions at the outputs. Consequently, the signal status as depicted at (iii) in Fig. 6 is obtained, where the constructive and destructive interference between the equal-amplitude RF contributions of the two arms result in the clear separation of the RHCP and LHCP signal at the two outputs. Moreover, the proposed modulation scheme prevents the undesired destructive interference of the optical carrier at the outputs, and simultaneously guarantees that after splitting at coupler κ_3, both outputs have their optical carriers in phase with the RF signals, resulting in optimal RF detection. Furthermore, it is straightforward to deduce that when this RF phase shift functionality is used in combination with unequal amplitude tapering between the two antenna components, the proposed polarization network will also be able to operates with signals with elliptic polarizations.

Similarly, this coherent optical processing principles can also be applied to DP signals with two orthogonal LPs. Figure 7 illustrates the processing steps. In this case, the polarization network only need to provide amplitude tapering functionality using coupler κ_4. Unlike the scheme for SP signals, this scheme allows arbitrary polarization rotation angle to be achieved optically. As illustrated in Fig. 7, one can change the sign of one output to its opposite by means of swapping the modulation formats between the two arms.

Moreover, for the transmission of DP signals, the inversed processing as for the receptions is required, where the MZMs and PDs should be swapped, and DSB-SC and DSB-FC modulation should be used for the two input RF signals separately. Then, it is straightforward to deduce that after the inversed processing as illustrated in Fig. 6 and Fig. 7, simultaneous DP transmissions will be achieved.

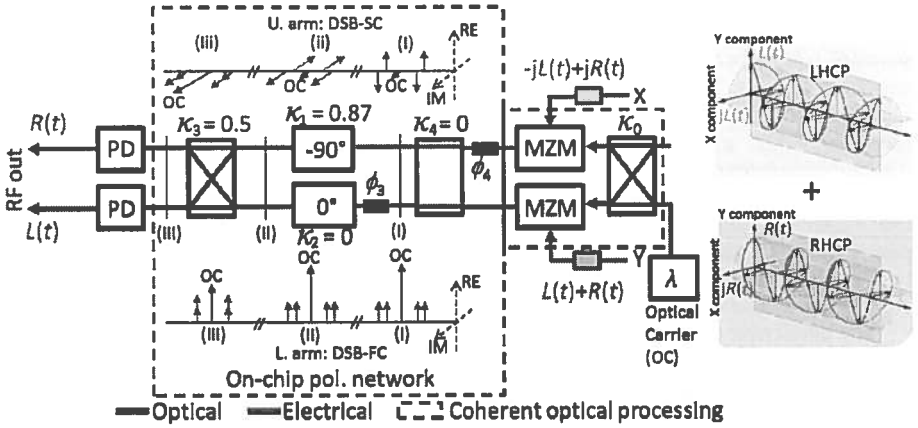

Fig. 6. System schemes for receive DLP antennas with CP signal radiations.

#181159 - $15.00 USD Received 4 Dec 2012; revised 23 Jan 2013; accepted 23 Jan 2013; published 1 Feb 2013

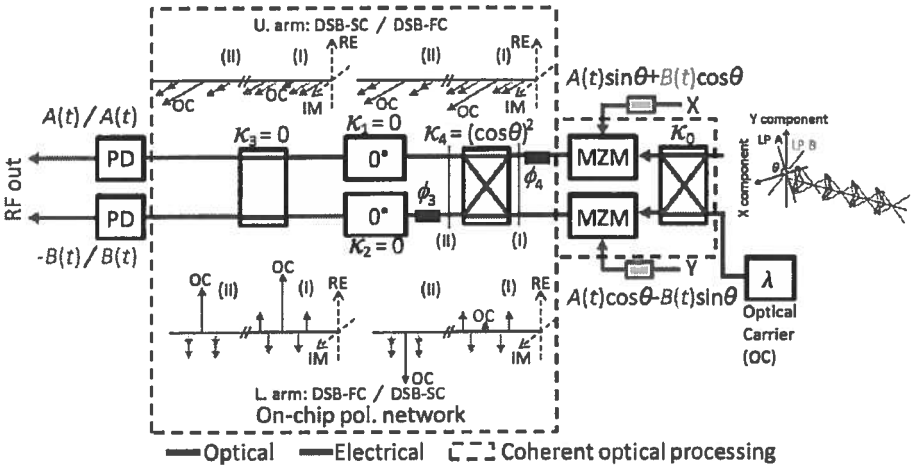

Fig. 7. System schemes for receive DLP antennas with LP signal radiations.

3. Device realization

The optical waveguide used for the fabrication of the integrated interleaver is TriPleX waveguide, a proprietary waveguide technology of LioniX B.V [22]. The waveguide is constructed with two strips of 170 nm-thick Si_3N_4 stacked on top of each other and separated physically by a 500 nm-thick SiO_2 intermediate layer, forming a "="-shaped cross-section. The cladding material surrounding the waveguide is also SiO_2, featuring a high-index-contrast characteristic. Figure 8(a) exhibits a photo of the waveguide cross-section. This double-strip waveguide geometry features a more fiber-resembling mode profile as well as an increased effective index of the optical mode in contrast to a conventional single-strip geometry. As a consequence, this improved mode profile compatibility and the increased mode confinement of the waveguide reduces the fiber-coupling loss and waveguide bend loss, respectively. The width of the Si_3N_4 strips is optimized to result in a single (TE-polarized) mode for C-band wavelengths (around 1550 nm). Moreover, the waveguide fabrication is compatible with standard equipment for CMOS process and uses low pressure chemical vapor depositions, which allows for low-cost and high-efficient productions, especially for high-volume scenarios. Worth to mention, this waveguide geometry has been characterized with a very low propagation loss of 0.1 dB/cm and simultaneously a small bend radius of 70 μm [23]. Besides, simulations have shown that by using a proper design of waveguide tapers at the chip facets, a fiber-chip coupling loss of 0.5 dB/facet is achievable. Therefore, TriPleX waveguide technology is considered to be an enabling photonic integrated circuit (PIC) platform for the realization of low-loss, on-chip complex MWP signal processors. For the interleaver chip of this paper, the taper design did not fully match the fibers pigtailed to the chip, and therefore a slightly larger insertion loss of 6 dB has been measured.

The interleaver was designed with a FSR of 20 GHz. Based on this and the group index of the waveguide (n_g = 1.72), the corresponding length difference between the two arms, ΔL = 8783 μm, and the roundtrip length of the RRs, $L_R = 2\Delta L$ = 17566 μm, were calculated and applied in the mask design of the interleaver. The optical couplers in the interleaver were implemented using MZI couplers, where the coupling coefficients can be varied by introducing an additional optical phase shift to one of the MZI arms. The reconfigurability of the interleaver was realized thermo-optically by means of resistor-based heaters on top of the waveguides. In this design, a total of 8 heaters are used to implement all the tuning elements as shown in Fig. 1(a). Figure 8(b) depicts the mask layout of the interleaver which has been fabricated. As it appears, the footprint of this mask is slightly smaller than 1 × 1 cm.

#181159 - $15.00 USD Received 4 Dec 2012; revised 23 Jan 2013; accepted 23 Jan 2013; published 1 Feb 2013

However, further footprint reduction is still possible, seeing the available spaces between the waveguides. This design was originally used as part of a complex optical beamformer chip [23]. For the sake of clarity, Fig. 8(b) excluded the structures of other functionalities, with the input and output waveguides of the interleaver extended and labeled for a good visibility.

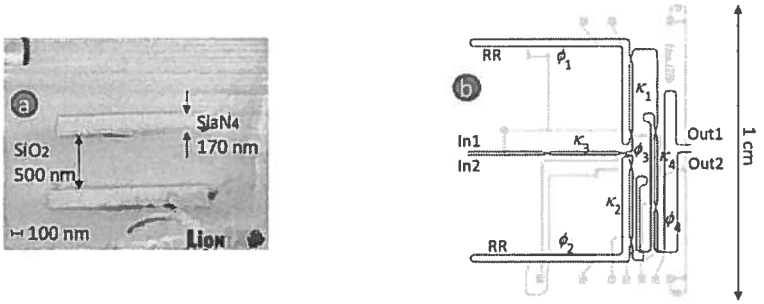

Fig. 8. Waveguide structure and mask layout deign of the interleaver: (a) scanning electron microscopy photo of waveguide cross-section, and (b) mask layout of the interleaver with waveguides in red, heaters in black, and leads in yellow.

4. Experimental verification of device functionalities

To verify the full reconfigurability and the MWP polarization network functionality of the fabricated interleaver, the experimental setup depicted in Fig. 9 was used for device characterizations. In this setup, an optical carrier was generated using a CW laser (EM4-253-80-057) driven by a low-noise current controller (1LX Lightwave LDX-3620); the modulating RF signal was generated by a vector network analyzer (Agilent NA5230A PNA-L); the modulation and detection were performed using a Mach-Zehnder intensity modulator (Avanex PowerLog FA-20) and a RF photodetector (Discovery semiconductor DSC30S), respectively; and the interleaver chip was controlled using a dedicated 12-bit heater controller.

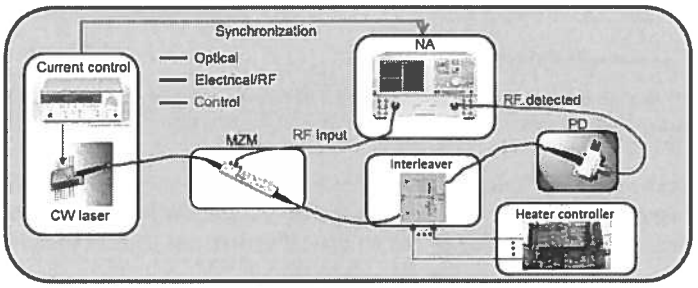

Fig. 9. Measurement setup for device characterizations.

For the measurement of the 5th-order filter responses of the interleaver, a current ramp is applied to the laser to perform a frequency sweep of the optical carrier over an FSR of the interleaver, and a RF signal with a frequency of 50 MHz was applied to the modulator, so that the filter responses can be measured using the network analyzer. To verify the design accuracy and full reconfigurability of the interleaver, multiple measurements were performed for different settings of the optical coefficients (κ_n's and ϕ_n's). Figure 10 demonstrates the measured optical power transmission, phase and group delay responses of the interleaver in comparison with the simulations. As it appears, the measured responses are in good agreement with the simulations. A small imbalance of the sidelobes is noticeable in Fig. 10(b) when the bar and cross port have symmetrical filter shape. This indicates that the fabricated

#181159 - $15.00 USD Received 4 Dec 2012; revised 23 Jan 2013; accepted 23 Jan 2013; published 1 Feb 2013

device has a small deviation from the desired path length relation, $L_R = 2\Delta L$, and consequently there is a limitation on the number of available channels for interleaver applicationss because the filter shape will become distorted as the frequency deviation increases. However, as demonstrated in Fig. 10, the fabricated device exhibits very good performance within a full FSR of 20 GHz. Furthermore, the measurement results in Fig. 11 verifies the full reconfigurability of the device, where changes in stopband suppression and shifts of the filter shape over one FSR are demonstrated by properly tuning the optical coefficients.

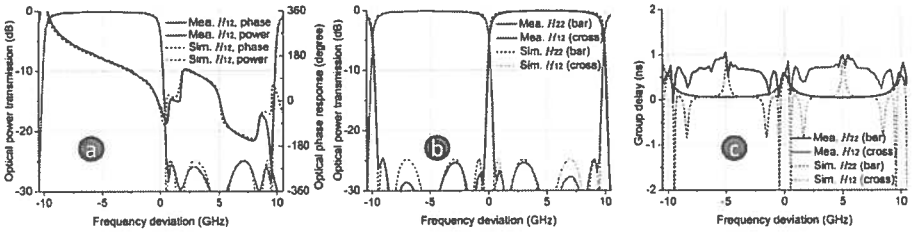

Fig. 10. Measured and simulated filter responses of the interleaver: (a) power transmission and phase response of H_{21}, (b) complementary nature of the two outputs of the interleaver, and (c) the corresponding group delay responses.

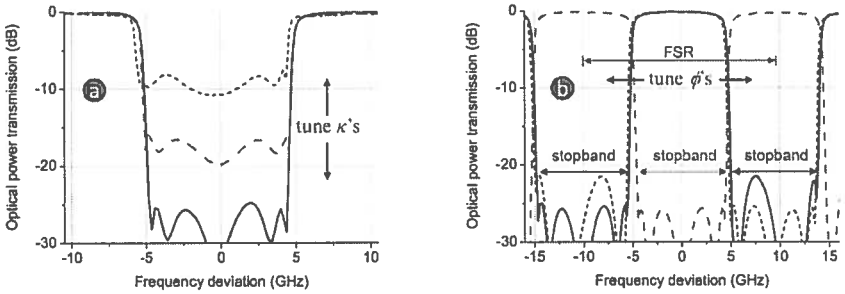

Fig. 11. Verification of full reconfigurability of the fabricated interleaver: (a) demonstration of changes in stopband suppression by varying κ's; and (b) demonstration of shifts of filter shape over one FSR.

Next, to verify the RF coupler functionalities for polarization network operations, network analyzer S_{21} measurements were performed to the device. For the RF measurements, $\kappa_3 = 0.5$ and $\kappa_4 = 0$ were applied to the device and an optical carrier was applied to the input port of the lower arm (In2), such that the RF responses of the two arms can be measured independently and clearly. The S_{21} reference was caliberated to the RF response of the upper arm with the RR decoupled ($\kappa_1 = 0$, the shortest optical path in the device). Then, as the HT functionality of a RR requires, the resonance frequencies of the RRs are aligned with the optical carrier [16]. The measured RF phase responses for the two settings of the RRs (as described in Section 2.2) are depicted in Fig. 12. As it appears, the reconfigurable 90°-phase-shift difference was achieved in a continuous bandwidth from 2 to 8 GHz, with an in-band phase ripple smaller than 5 degree. The corresponding RF magnitude responses are flat over this bandwidth as explained in [16], and slight magnitude differences due to the additional loss of the RRs can be compensated by adjusting the optical coupler κ_3. Hereby, the optical and RF measurement results prove that when used for MWP signal processing, the interleaver is able to serve as a wideband 2 × 2 RF coupler with reconfigurable complex coefficients, and therefore can be used for RF applications such as wideband polarization networks. Moreover,

#181159 - $15.00 USD Received 4 Dec 2012; revised 23 Jan 2013; accepted 23 Jan 2013; published 1 Feb 2013

the frequency periodicity of the device allows it to operate in multiple frequency bands spaced by the FSR of the RRs, 10 GHz in this example, and the in-band phase ripple can be further reduced for lower bandwidth-FSR ratios. In practice, these bandwidth-related characteristics are scalable with different FSR designs.

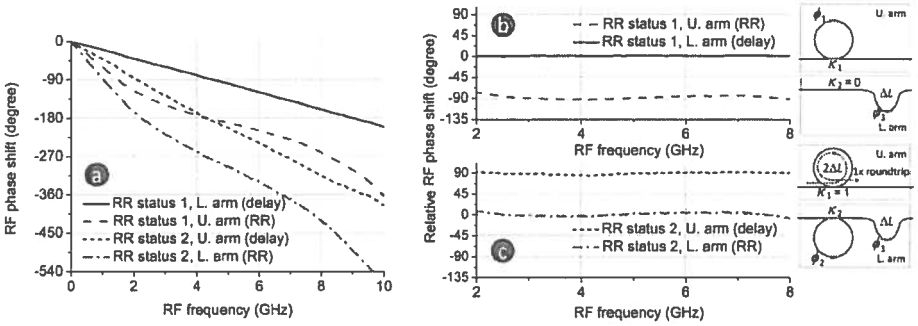

Fig. 12. Measurements of complex coefficients of the polarization network: (a) RF phase measurements of the two arms for two different status of the RRs, (b)-(c) corresponding quadrature RF phase relations between the two arms. Inset: illustrations of the two different status of the RRs.

5. Conclusions

In this paper, a novel on-chip wideband MWP 2 × 2 RF coupler is proposed and demonstrated, in association with discussions on its application possibilities as a RF polarization network for wideband DLP antennas. This 2 × 2 RF coupler is implemented using a waveguide-based optical interleaver which consists of a two-ring resonator-assisted asymmetric MZI structure. This structure features simplicity and compactness. The full reconfigurability of the device enables the achievement of the desired complex coefficients for various polarization network operations. The proposed device can equip the DLP antennas with not only polarization rotation capability for linear polarization LP scenarios but also the capability to operate with and switch between two opposite CPs, namely between LHCP and RHCP. Operating together with a particular modulation scheme, the device is also able to serve for simultaneous feeding of DP signals. These photonic-implemented RF functionalities can be applied to wideband antenna systems to perform agile polarization manipulations and trackings. An example of such an interleaver was fabricated in TriPleX waveguide technology, with a FSR of 20 GHz. The fabricated device exhibited a very good interleaver performance, and demonstrated a continuous RF bandwidth from 2 GHz to 8 GHz, with an in-band phase ripple smaller than 5 degree. However, this bandwidth is scalable with different FSR designs, and the frequency periodicity of the device allows this bandwidth to be available in multiple equally-spaced frequency bands, 10 GHz in this example. The waveguide-based structure allows the device to be integrated with other functional building blocks on a PIC to create various on-chip complex MWP signal processors. Of particular interest, it can be included in an optical beamformer for phased array antennas, so that simultaneous wideband beam and polarization trackings can be achieved photonically. To our knowledge, this is the first-time on-chip demonstration of an integrated microwave photonic polarization network for DLP antennas.

Acknowledgment

The research described in this paper is carried out within the Dutch Point One R&D Innovation Project: Broadband Satellite Communication Services on High-Speed Vehicles, with project number PNE101008. The authors are thankful to Agentschap NL for financing the project.